COUPLED REACTION AND FLOW IN SUBDUCTION ZONES: SILICA METASOMATISM IN THE MANTLE WEDGE

8

Craig E. Manning

8.1 INTRODUCTION

Large quantities of H_2O are carried to great depth during subduction of sediment and hydrated oceanic crust. Much of this H_2O is bound in hydrous minerals. When dehydration reactions proceed, the liberated fluid may migrate back up the slab or into the overlying mantle wedge (e.g. Peacock, 1990a, 1993a,b; Bebout, 1991a,b). Regardless of the fluid's trajectory, the strong dependence of mineral solubility on pressure and temperature suggests that this flow may lead to extensive metasomatism. This is supported by field and analytical data, which show that metasomatic redistribution of elements is common in subduction-zone settings (Moore, Liou and King, 1981; Wyllie and Sekine, 1982; Tatsumi, Hamilton and Nesbitt, 1986; Sorenson and Barton, 1987; Sorenson, 1988; Bebout and Barton, 1989, 1993). Metasomatism ultimately modifies the composition of the mantle above subduction zones and may exert a first-order control on the genesis of arc magmas. Understanding metasomatism in subduction zones is therefore important for gaining insight into crustal evolution, magma genesis and element cycling.

Limited experimental data for mineral solubility at high pressures have prevented numerical modelling of major-element transport during fluid flow and mineral reaction in subduction zones. However, new experimental results on the solubility of quartz to high pressures (Manning, 1994) allow simple one-dimensional models of Si redistribution at conditions appropriate to subduction zones. Here, Si metasomatism in the hanging wall above a subducting slab (mantle wedge) is evaluated. This analysis illustrates the combined controls of fluid flux and phase equilibria on material transport, and places constraints on the extent of Si metasomatism that may be expected in long-lived, steady-state subduction zones.

8.2 BACKGROUND

Fluid–rock interaction in the mantle wedge can be modelled in simplified form using the system $MgO–SiO_2–H_2O$ (MSH), which approximates the bulk composition of the depleted mantle typically present in oceanic convergent margins. Thermodynamic calculations employed equations and data of Haar, Gallagher and Kell (1984), Berman *et al.* (1986), Berman (1988) and Manning (1994). Thermodynamic properties of the fluid phase were taken to be those of pure H_2O.

Phase relations in the MSH system were computed using model steady-state thermal regimes for subduction at 10 cm a^{-1}, an angle of 20°, and rock densities of 3.0 g cm^{-3} (Peacock, 1993a). The change in pressure with temperature, or P–T path, corresponds to the slab–mantle interface to a vertical depth of *c.* 70 km, or *c.* 200 km of slab length. The four simulated P–T paths shown in Fig. 8.1 differ in that temperature at a given

depth decreases from Path 1 through Path 4. In Peacock's (1993a) simulations, these temperature differences were attained using shear stresses of 100 MPa, 67 MPa, 33 MPa and 0 MPa for Paths 1 through 4, respectively. The actual shear stresses in subduction zones are uncertain and may vary; the paths simply illustrate the range in P–T conditions which may result from different subduction scenarios. For example, Path 1 represents the P–T regime that might be expected when young oceanic crust is subducted, whereas Path 3 probably best reflects conditions likely in a long-lived, steady-state subduction zone. Predicted P–T paths vary with model conditions and parameters (Peacock, 1992a, 1993a; Peacock, Rushmer and Thompson, 1994; Davies and Stevenson, 1992), but the paths used here provide a simple framework for illustrating the effect of pressure, temperature and bulk composites on aqueous silica transport.

8.3 PHASE RELATIONS AND $SiO_{2(aq)}$ CONCENTRATION

Measured quartz solubilities at high pressures and temperatures allow prediction of the concentration of Si in H_2O in equilibrium with quartz from 25°C, 1 bar to > 20 kbar and *c.* 1000°C (Manning, 1994). Si contents of pure H_2O at quartz saturation are shown as a function of P and T in Fig. 8.1 with the representative P–T paths. Quartz solubility along the P–T paths increases with increasing pressure and temperature by 10^3 to 10^5 times. Maximum solubilities are attained at the greatest depth and range from 0.16 mol kg^{-1} H_2O (Path 3) to 6.6 mol kg^{-1} H_2O (Path 1). Material transport by aqueous solutions is governed by both the magnitude of solubility as well as solubility gradients. Thus, for quartz-bearing lithologies (i.e. metasediments and metabasalts), the greatest potential for Si redistribution exists in the deep portions of subduction zones where there are high solubilities and large changes in solubility with distance (Manning, 1996a,b). The greatest potential for Si transport will therefore exist in subduction zones where conditions favour high temperatures. Examples include the subduction of hot young oceanic crust, young subduction zones and high rates of shear heating.

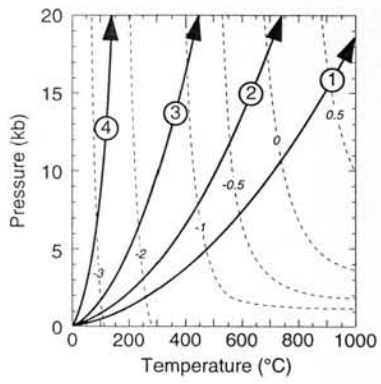

Figure 8.1 Isopleths of log $m_{SiO_{2(aq)}}$ in equilibrium with quartz as a function of pressure and temperature. Calculated using the equation of Manning (1994). P–T paths 1–3 (bold arrows) from Peacock (1993a) (see text).

The concentration of $SiO_{2(aq)}$ in equilibrium with quartz (Fig. 8.1) can be used to analyse metasomatic phase relations. This can be seen from the equilibrium between pure quartz and aqueous silica,

$$\underset{\text{quartz}}{SiO_2} = SiO_{2(aq)} \qquad (8.1)$$

which at constant pressure and temperature requires that

$$\Delta G^\circ_{SiO_{2(aq)}} = \Delta G^\circ_{\text{quartz}} - RT \ln a_{SiO_{2(aq)}} \qquad (8.2)$$

where ΔG° is the standard molal Gibbs free energy difference between a reference state (25°C, 1 bar) and the P and T of interest, R is the gas constant, a is activity. Standard states for minerals and water are the pure phase at any pressure and temperature; the standard state for aqueous silica is unit activity of the species in a hypothetical one molal solution at infinite dilution and the pressure and temperature of interest. The activity of $SiO_{2(aq)}$ is closely approximated by its molality (m) because Si forms a neutral hydrated species with an activity coefficient of unity over a wide range in pH (Walther and Helgeson, 1977).

Equation 8.2 thus becomes

$$\Delta G^\circ_{SiO_{2(aq)}} = \Delta G^\circ_{quartz} - RT \ln m_{SiO_{2(aq)}} \quad (8.3)$$

This allows calculation of the standard molal Gibbs free energy of aqueous silica which can be combined with thermodynamic data for minerals and H_2O to determine phase relations as a function of silica concentration in the fluid. For example, the equilibrium between forsterite and enstatite

$$\underset{\text{forsterite}}{Mg_2SiO_4} + SiO_{2(aq)} = \underset{\text{enstatite}}{2MgSiO_3} \quad (8.4)$$

leads to

$$\ln m_{SiO_{2(aq)}} = -\frac{\Delta G^\circ_{(8.4)}}{RT} = -\frac{2\Delta G^\circ_{en} - \Delta G^\circ_{fo} - \Delta G^\circ_{SiO_{2(aq)}}}{RT} \quad (8.5)$$

where $\Delta G^\circ_{(8.4)}$ is the difference between standard molal Gibbs free energies of reactants and products for equilibrium 8.4.

Figure 8.2 shows results of these calculations in the system $MgO-SiO_2-H_2O$ for Path 3. This path provides a reasonable approximation of steady-state conditions experienced by a long-lived subduction zone. Figure 8.2 is similar to diagrams given by Hemley *et al.* (1977a,b) and Evans and Guggenheim (1988), except that pressure and temperature vary along the ordinate. The maximum molality of $SiO_{2(aq)}$ is defined by quartz saturation and this maximum Si content increases between 0 and 70 km depth by *c.* 1000 times. Coexisting MSH mineral pairs fix $m_{SiO_{2(aq)}}$ at constant P and T and buffer $m_{SiO_{2(aq)}}$ along phase boundaries as P and T change along a specified path. The width of one-phase fields defines the range in Si concentration over which the phase is stable. These fields therefore indicate regions in which $m_{SiO_{2(aq)}}$ may vary at a given position in subduction zones. At $P > 6$ kbar, talc is stable with quartz at the highest $m_{SiO_{2(aq)}}$; as $m_{SiO_{2(aq)}}$ decreases, antigorite and then brucite become stable with the fluid phase. Chrysotile is stable with respect to antigorite + brucite below 6 kbar and at $m_{SiO_{2(aq)}}$ between brucite and antigorite.

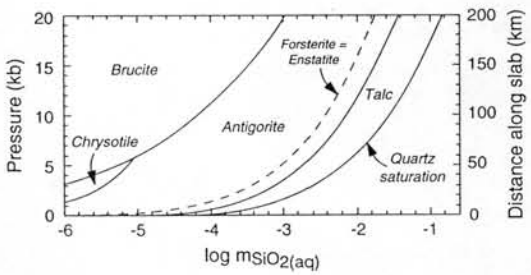

Figure 8.2 Phase relations in the system $MgO-SiO_2-H_2O$ as a function of $SiO_{2(aq)}$ concentration (mol kg^{-1} H_2O) and pressure for Path 3. Temperature varies with pressure along the ordinate (Fig. 8.1). Solid curves represent stable equilibria; the dashed curve denotes metastable forsterite–enstatite equilibrium in the presence of H_2O. The maximum equilibrium $m_{SiO_{2(aq)}}$ is defined by quartz saturation; fluids with greater Si contents are metastably supersaturated with respect to quartz.

Lizardite is not included in the calculations because the thermodynamic properties of the Al-free end-member are poorly known. Field evidence suggests lizardite is a stable serpentine polymorph (Wicks and O'Hanley, 1988); however, all experimental syntheses (e.g. Chernosky, 1975) appear to be metastable with respect to antigorite and chrysotile, which implies that Al-free lizardite can only be stable at low temperatures (e.g. < 250°C at 2 kbar; Chernosky, Berman and Bryndzia, 1988). Thus, natural occurrences of lizardite likely reflect low temperatures or stabilization by minor Al substitution into the crystal structure. Because of the higher temperatures and Al-free bulk composition considered here, lizardite will not be considered further.

Figure 8.2 shows for reference the metastable equilibrium between forsterite + enstatite, which is the model mineral assemblage of depleted, harzburgitic oceanic mantle in the MSH system. Both minerals are unstable with H_2O below 20 kbar along Path 3. The stable mineral assemblage in the presence of H_2O is governed by the relative abundance of forsterite and enstatite. At 25°C, 1 bar, a model harzburgite composed of $\geqslant 59$ vol% forsterite ($\leqslant 41$ vol% enstatite) will contain chrysotile + brucite when fully hydrated.

Harzburgites with modal volumes of 59–49 vol% forsterite will hydrate to chrysotile + antigorite, whereas forsterite contents of <49 vol% will result in antigorite + talc upon hydration. Above *c.* 6 kbar, fully hydrated harzburgite will consist of antigorite + brucite (Fig. 8.2) for original forsterite content $\geqslant 49$ vol%, and antigorite + talc for lower original forsterite abundance.

The variation in hydrated mineral assemblages as a function of bulk composition is important because slight differences in bulk SiO_2 content can result in quite different Si concentrations in the coexisting fluid phase, which may lead to contrasting magnitudes of Si mass transport. For example, at the slab–mantle interface at 20 kbar along Path 3, a fully hydrated harzburgite originally containing 48 vol% forsterite, or 51.60 wt% SiO_2, will consist of antigorite + talc in equilibrium with a fluid in which $\log m_{SiO_{2(aq)}} = -1.2$, whereas an original forsterite content of 49 vol%, or 51.42 wt% SiO_2, will result in antigorite + brucite coexisting with a fluid with $\log m_{SiO_{2(aq)}} = -3.0$. Thus, the 0.18 wt% variation in bulk SiO_2 results in $m_{SiO_{2(aq)}}$ values which differ by a factor of 63. Migration of these two fluids will clearly result in contrasting magnitudes of Si redistribution.

8.4 COUPLED REACTION AND FLOW IN THE MANTLE WEDGE

8.4.1 CONCEPTUAL MODEL

After sufficient time has elapsed since the inception of subduction, a steady-state metasomatic mineral zonation will exist in the mantle wedge with increasing distance from the slab. The conceptual model for this scenario is illustrated in Fig. 8.3. As subducting oceanic lithosphere and sediment pass beneath the mantle wedge, a portion of the fluid liberated during devolatilization reactions in the slab will enter the overlying plate with a subvertical trajectory. Solubility of Mg is likely to be low in the absence of Cl and at near-neutral pH, so the fluid in the model system can be assumed to have two components, SiO_2 and H_2O.

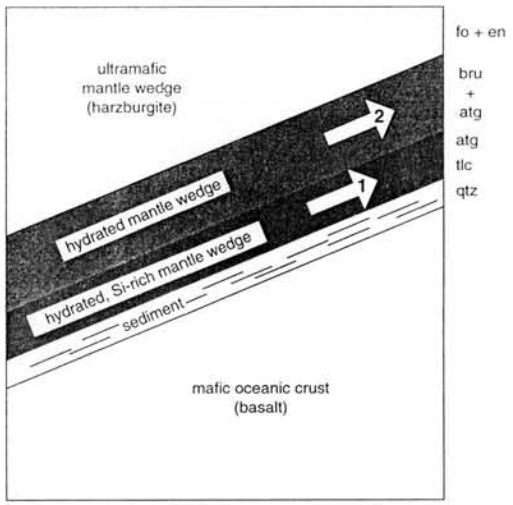

Figure 8.3 Conceptual model of up-dip fluid flow in the mantle wedge above a subducting slab. Mineral assemblages on the right are inferred from Fig. 8.2. Arrows denote trajectories of flow for the two cases examined (see text).

Sediments are likely to buffer fluid composition at or near quartz saturation (Manning, 1995a,b), fixing $m_{SiO_{2(aq)}}$ at its maximum value at the slab–mantle interface. As the H_2O–SiO_2 fluid migrates into the mantle wedge it will react with forsterite and enstatite such that a hydrous, Si-enriched region will develop near the slab–mantle interface. Within several kilometres of the slab this can be assumed to occur isothermally and isobarically for lithospheric mantle at the steady-state conditions of Path 3. Isobaric, isothermal flow from the slab to the mantle will correspond to a horizontal path of decreasing $SiO_{2(aq)}$ concentration in Fig. 8.2. Because of the low SiO_2/H_2O ratio of the fluid, the SiO_2 content will rapidly become buffered by the mantle through precipitation of talc and antigorite. Thus, continued upward flow will hydrate metastable forsterite + enstatite to antigorite + brucite, but not modify the Si content of the mantle significantly. The steady-state mineral zonation with increasing distance from the slab will be talc → talc + antigorite → antigorite → antigorite + brucite → forster-

ite + enstatite at pressures greater than those of the chrysotile–antogorite–brucite invariant point (Fig. 8.2).

Bouyancy forces on the fluid lead to upward flow, a significant component of which may be parallel to the slab–mantle interface in the mantle wedge. At local equilibrium different mineral assemblages impose contrasting values of $m_{SiO_{2(aq)}}$ which change with P and T (Fig. 8.2). Thus, flow of an H_2O–SiO_2 fluid will cause redistribution of Si, and the extent of this redistribution will depend on the starting bulk composition as defined by the portion of the mantle in which the flow occurs. Depleted diopside-free oceanic harzburgites typically have modal volumes of orthopyroxene of 15–20% if spinel is ignored (e.g. Dick, Fisher and Bryan, 1984), so the stable MSH mineral assemblage in the presence of H_2O at high pressure will be antigorite + brucite. However, near the slab mantle interface, Si-rich aqueous fluids may increase the SiO_2 content of the mantle sufficiently to stabilize talc (e.g. Bebout and Barton, 1993). Two cases are therefore examined: (1) flow in the hydrated and metasomatized region near the slab–mantle interface in which the Si content has been increased during slab devolatilization; and (2) flow in the hydrated portion of the mantle wedge in which the starting Si content is that of unaltered harzburgite.

8.4.2 NUMERICAL MODEL

The number of moles of SiO_2 (n_{SiO_2}) produced or consumed as a consequence of fluid-driven reaction may be determined from an analytical solution for coupled one-dimensional flow and reaction (Baumgartner and Ferry, 1991):

$$n_{SiO_2} = \frac{q_m}{(1 - X_{SiO_2}\Sigma(\nu_J/\nu_{SiO_2}))}\frac{dX_{SiO_2}}{dz} \qquad (8.6)$$

where X_{SiO_2} is the mole fraction of SiO_2 in the fluid phase, z is distance along the flow path, ν is the stoichiometric coefficient of the jth species for an equilibrium of interest, and q_m is time-integrated molar fluid flux defined by

$$q_m = q_m^0\left[1 + \frac{(X_{SiO_2} - X^0_{SiO_2})(1 + \nu_{H_2O}/\nu_{SiO_2})}{1 - X_{SiO_2}(1 + \nu_{H_2O}/\nu_{SiO_2})}\right] \qquad (8.7)$$

where q_m^0 and $X^0_{SiO_2}$ are initial time-integrated molar flux and SiO_2 mole fraction, respectively. Because the derivative in equation 8.6 is determined by relations shown in Figs 8.1 and 8.2, equations 8.6 and 8.7 allow calculation of the number of moles of SiO_2 consumed or liberated by a given reaction for a specified time-integrated fluid flux.

In each case examined, fluid migrated up-dip such that P and T decreased with increasing distance along the flow path. Flow was assumed to begin at a depth of *c.* 70 km, or 20 kbar and 450°C (Fig. 8.1). The length of the flow path was *c.* 210 km; i.e. the length along the slab from the point at which flow begins to the earth's surface. Calculations were performed in a constant MgO reference frame, so rock volume varies along the flow path, and enthalpies of reaction were ignored in the energy balance implicit in the assumption of a constant temperature gradient (cf. Ferry, 1995; Hanson, 1995).

8.4.3 RESULTS

The first case examined is flow in the hydrated, Si-metasomatized portion of the mantle wedge near the slab–mantle interface (lower arrow, Fig. 8.3). A starting mineral assemblage of antigorite with an infinitesimal amount of talc was assumed, yielding a bulk composition with 45.0 wt% SiO_2. The presence of talc has an insignificant influence on bulk composition, but it means that $SiO_{2(aq)}$ will be buffered by the equilibrium

$$\underset{\text{antigorite}}{Mg_{48}Si_{34}O_{85}(OH)_{62}} + 30SiO_{2(aq)} = \underset{\text{talc}}{16Mg_3Si_4O_{10}(OH)_2} + 15H_2O \qquad (8.8)$$

Because the production of talc from antigorite H_2O, q_m increases along the flow path; however, $SiO_{2(aq)}$ mole fractions are low, so the magnitude

of this increase is vanishingly small. At the inlet at 20 kbar, $m_{SiO_{2(aq)}}$ is fixed at 0.040 mol kg^{-1} H_2O by talc–antigorite equilibrium (Fig. 8.2). Up-dip flow requires that $SiO_{2(aq)}$ concentration decreases (Fig. 8.2), which is accomplished by the production of talc and consumption of antigorite. Changes in modal % talc produced for specified q_m^0 at the inlet are shown in Fig. 8.4a. For time-integrated molar flux $> 10^6$ mol cm^{-2}, more than several tenths volume % of talc will form from antigorite as a consequence of the flow of Si-bearing fluid. At any point along the flow path, the amount of talc produced increases with q_m^0 because of the greater quantities of advected Si. The magnitude of talc production decreases along the flow path because the magnitude of the change in Si solubility decreases as pressure diminishes (Fig. 8.2). Figure 8.4b illustrates that bulk SiO_2 content increases with the amount of talc produced. The maximum SiO_2 content that can be achieved corresponds to 100% talc. When all antigorite has been converted to talc, $m_{SiO_{2(aq)}}$ is no longer constrained by the talc–antigorite phase boundary, and $m_{SiO_{2(aq)}}$ will be greater than that imposed by antigorite until the antigorite–talc phase boundary is intersected downstream (up-dip).

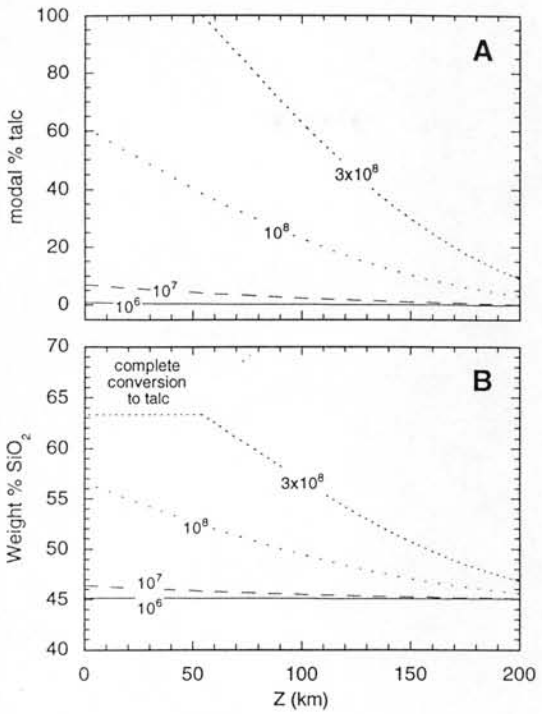

Figure 8.4 (a) Variation in modal % talc with distance along flow path in hydrated, Si-metasomatized mantle wedge. Curves are labelled with time-integrated molar fluxes at the inlet. (b) Variation in bulk rock SiO_2 content with distance along flow path. The maximum values attained correspond to complete conversion to talc.

The second case examined is flow in the hydrated but unmetasomatized portion of the mantle wedge (upper arrow, Fig. 8.3). As noted above, the model anhydrous assemblage (forsterite ≫ enstatite) is unstable in the presence of H_2O with respect to antigorite + brucite and chrysotile + brucite at all points along Path 3. An assumed starting mode of 85% forsterite, 15% enstatite would result in 84.2% antigorite, 15.8% brucite when fully hydrated using molar volumes at 25°C, 1 bar. Initially, $SiO_{2(aq)}$ concentration will be fixed by the equilibrium

$$\underset{\text{brucite}}{48Mg(OH)_2} + 34SiO_{2(aq)} = \underset{\text{antigorite}}{Mg_{48}Si_{34}O_{85}(OH)_{62}} + 17H_2O \qquad (8.9)$$

However, at low pressures beyond *c.* 150 km along the flow path (less than *c.* 6 kbar), the stable mineral assemblage becomes chrysotile + brucite, and equilibrium 8.9 is replaced by

$$\underset{\text{brucite}}{3Mg(OH)_2} + 2SiO_{2(aq)} = \underset{\text{chrysotile}}{Mg_3Si_2O_5(OH)_4} + H_2O \qquad (8.10)$$

(Fig. 8.2). The value of $m_{SiO_{2(aq)}}$ is fixed at the inlet at *c.* 0.001 mol kg^{-1} H_2O by equilibrium 8.9. Figure 8.2 shows that up-dip migration of this fluid in the deep part of the mantle wedge requires that $m_{SiO_{2(aq)}}$ decreases in equilibrium with antigorite + brucite. This will be accomplished by production of antigorite and consumption of brucite. When antigorite becomes metastable with respect to chrysotile in the presence of brucite, chrysotile will be produced as brucite is consumed. Both equilibria are dehydration reactions, so the consumption of SiO_2 leads to the production of H_2O, and q_m will increase slightly along the flow path.

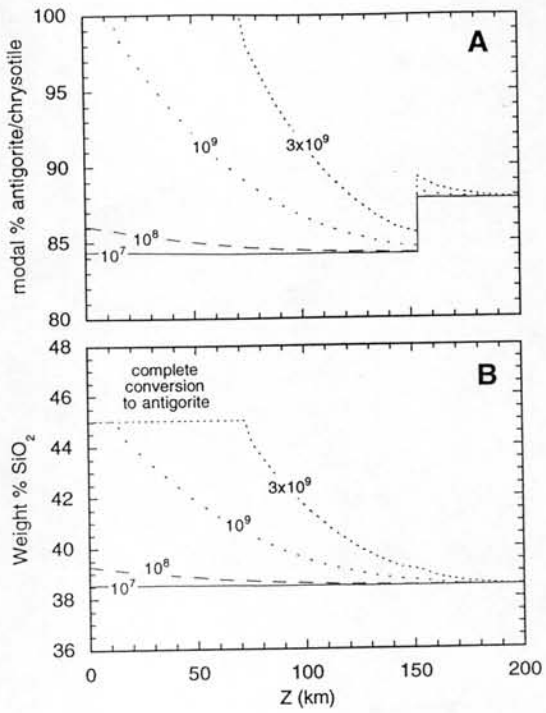

Figure 8.5 (a) Variation in modal % antigorite or chrysotile with distance along flow path in hydrated, unmetasomatized mantle wedge. Curves are labelled with time-integrated molar fluxes at the inlet. The discontinuity at *c.* 150 km reflects the reaction of antigorite and brucite to chrysotile (equilibrium 8.10). (b) Variation in bulk rock SiO_2 content with distance along flow path. The maximum values attained correspond to complete conversion to antigorite.

Changes in the modal % antigorite and chrysotile along the flow path for specified time-integrated molar fluxes (q_m^0) in mol fluid cm^{-2} rock are shown in Fig. 8.5a. For any given molar flux above 10^7 mol cm^{-2}, the mineral assemblage will be detectably modified by the flow of fluid. As with the first case, the abundance of secondary minerals produced by fluid flow increases with q_m^0 at any point along the flow path, but decreases up-dip at constant q_m^0. However, the flux isopleths differ from those in Fig. 8.4 in that all flux isopleths have a discontinuity at *c.* 150 km where antigorite reacts with brucite to produce chrysotile. The effect of the change in mineral mode due to Si addition to the rock is illustrated in Fig. 8.5b. The formation of antigorite and chrysotile from brucite and fluid translates to increases in bulk SiO_2 by several wt%. At $q_m^0 > 8 \times 10^8$ mol cm^{-2} all brucite is consumed at some point along the flow path, and the fluid composition is no longer constrained by a two-phase assemblage. As in the first case, this condition will hold until the fluid intersects the antigorite–brucite phase boundary downstream (up-dip).

8.5 DISCUSSION

Figures 8.4 and 8.5 show that if there is a component of fluid flow in the mantle wedge that is subparallel to the slab–mantle interface, Si will be advected from depth toward the earth's surface, regardless of mantle mineral assemblage. The extent of advection depends on the magnitude of the time-integrated fluid flux. In metasomatized hydrous mantle near the slab (Fig. 8.4), flow of $> 10^6$ mol cm^{-2} leads to observable increases in bulk SiO_2 content. In unmetasomatized hydrous mantle, ten times more fluid is required to produce similar increases in bulk SiO_2. The predicted metasomatic changes in bulk SiO_2 content are greatest in the deepest parts of subduction zones, where solubilities and solubility gradients are largest.

The hydrological implications of the calculations can be appreciated by placing conservative bounds in the Darcy velocities and permeabilities required to produce Si metasomatism by porous flow in the mantle wedge. Steady-state subduction may persist for many tens of million years. For 50 million years of subduction, the minimum integrated molar fluxes of 10^6 to 10^7 mol cm^{-2} required to generate significant large-scale Si metasomatism in steady-state subduction zones correspond to minimum time-averaged Darcy velocities of 9.5×10^{-11} to 9.5×10^{-10} m s^{-1} assuming an H_2O volume of 15 cm^3 mol^{-1} at the flow inlet. These Darcy velocities require time-averaged matrix permeabilities in excess of 1.6×10^{-18} m^2 for a fluid pressure gradient along the flow path

ACKNOWLEDGEMENTS

Supported by NSF EAR-9405999. I thank Lukas Baumgartner and Simon Peacock for insightful reviews. An early draft of the manuscript was improved by D. Rothstein, K. Knesel and H. Lin.

REFERENCES

Baumgartner, L. P. and Ferry, J. M. (1991) A model for coupled fluid-flow and mixed-volatile mineral reactions with applications to regional metamorphism. *Contributions to Mineralalogy and Petrology*, **106**, 273–85.

Bebout, G. E. (1991a) Geometry and mechanisms of fluid flow at 15 to 45 kilometer depths in an early Cretaceous accretionary complex. *Geophysical Research Letters*, **18**, 923–6.

Bebout, G. E. (1991b) Field-based evidence for devolatilization in subdivision zones: implications for arc magmatism. *Science*, **251**, 413–16.

Bebout, G. E. and Barton, M. D. (1989) Fluid flow and metasomatism in a subduction zone hydrothermal system: Catalina Schist terrane, California. *Geology*, **17**, 976–80.

Bebout, G. E. and Barton, M. D. (1993) Metasomatism during subduction: Products and possible paths in the Catalina Schist, California. *Chemical Geology*, **108**, 61–92.

Berman, R. G. (1988) Internally-consistent thermodynamic data for minerals in the system Na_2O–K_2O–CaO–MgO–FeO–Fe_2O_3–Al_2O_3–SiO_2–TiO_2–H_2O–CO_2. *Journal of Petrology*, **29**, 445–522.

Berman, R. G., Engi, M., Greenwood, H. J. and Brown, T. H. (1986) Derivation of internally-consistent thermodynamic data by the technique of mathematical programming: A review with application to the system MgO–SiO_2–H_2O. *Journal of Petrology*, **27**, 1331–64.

Chernosky, J. V. (1975) Aggregate refractive indices and unit cell parameters of synthetic serpentine in the system MgO–Al_2O_3–SiO_2–H_2O. *American Mineralogist*, **60**, 200–8.

Chernosky, J. V., Berman, R. G. and Bryndzia, L. T. (1988) Stability, phase relations, and thermodynamic properties of chlorite and serpentine group minerals, in *Hydrous Phyllosilicates (Exclusive of Micas)* (ed. S. W. Bailey), Reviews in Mineralogy, **19**, 293–346.

Davies, J. H. and Stevenson, D. J. (1992) Physical model of source region of subduction zone volcanics. *Journal of Geophysical Research*, **97**, 2037–70.

Dick, H. J. B., Fisher, R. L. and Bryan, W. B. (1984) Mineralogic variability of the uppermost mantle along mid-ocean ridges. *Earth and Planetary Science Letters*, **69**, 88–106.

Ernst, W. G. (1990) Thermobarometric and fluid expulsion history of subduction zones. *Journal of Geophysical Research*, **95**, 9047–53.

Evans, B. W. and Guggenheim, S. (1988) Talc, pyrophyllite, and related minerals, in *Hydrous Phyllosilicates (Exclusive of Micas)* (ed. S. W. Bailey), Reviews in Mineralogy, **19**, 225–94.

Ferry, J. M. (1995) Reply to comment by R. Brooks Hanson on "Role of fluid flow in the contact metamorphism of siliceous dolomitic limestones". *American Mineralogist*, **80**, 1226–8.

Grove, M. and Bebout, G. E. (1995) Jurassic and Cretaceous tectonic evolution of coastal southern California: Insights from the Catalina schist. *Tectonics*, **14**, 1290–1308.

Haar, L., Gallagher, J. S. and Kell, G. S. (1984) *NBS/NRC Steam Tables*, Hemisphere, New York.

Hanson, R. B. (1995) Comment on "Role of fluid flow in the contact metamorphism of siliceous dolomitic limestones" by John M. Ferry: Conservation of energy in applications of reaction-flow models. *American Mineralogist*, **80**, 1222–5.

Hemley, J. J., Montoya, J. W., Christ, C. L. and Hostetler, P.B. (1977a) Mineral equilibria in the MgO–SiO_2–H_2O system: I Talc–chrysotile–forsterite–brucite stability relations. *American Journal of Science*, **277**, 322–51.

Hemley, J. J., Montoya, J. W., Shaw, D. R. and Luce, R. W. (1977b) Mineral equilibria in the MgO–SiO_2–H_2O system: II Talc–antigorite–forsterite–anthophyllite–enstatite stability relations and some geologic implications in the system. *American Journal of Science*, **277**, 322–51.

Manning, C. E. (1994) The solubility of quartz in H_2O in the lower crust and upper mantle. *Geochimica et Cosmochimica Acta*, **58**, 4831–9.

Manning, C. E. (1996a) Effect of sediments on aqueous silica transport in subduction zones, in *Dynamics of Subduction* (eds G. E. Bebout *et al.*), American Geophysical Union Monograph, in press.

Manning, C. E. (1996b) Phase-equilibrium controls on SiO_2 metasomatism by aqueous fluid in subduction zones: reaction at constant pressure and temperature. *International Geology Review*, submitted.

Moore, D. E., Liou, J. G. and King, B.-S. (1981) Chemical modifications accompanying blueschist facies metamorphism of Franciscan conglomerates, Diablo Range, California. *Chemical Geology*, **33**, 237–63.

of 1.8×10^4 Pa m^{-1} and a dynamic viscosity of 3×10^{-4} kg m^{-1} s^{-1}. Although viscosity is poorly known at the conditions of this study, its pressure-dependence is small at high pressures (Haar, Gallagher and Kell, 1984), so uncertainties in this property will not effect calculated permeability strongly. Also, the value used is likely to be a minimum, consistent with the calculation of the minimum permeability required to produce Si metasomatism.

The minimum Darcy velocities and permeabilities that would be implied by Si metasomatism in the mantle wedge are large compared to those thought to be associated with crustal-scale flow systems during model metamorphic events (e.g. 10^{-12} to 10^{-11} m s^{-1}, Thompson and Connolly, 1992). However, large fluxes may not be unreasonable in view of the large quantities of fluid continuously carried downward in the slab. For example, for a subduction rate of 10 cm a^{-1}, Peacock (1990b) calculated fluid production at distances >200 km along model slabs which correspond to Darcy velocities across the slab–mantle interface of up to 2×10^{-10} m s^{-1} for different ages of crust and dehydration scenarios, and assuming a fluid density of 1000 kg m^{-3}. Flow of this fluid up-dip would be sufficient to cause minor redistribution of Si in the mantle wedge (Figs 8.4 and 8.5).

Such estimates depend strongly on the choice of subduction parameters, and our limited knowledge of the hydrological and metamorphic processes at depth in convergent margins makes it difficult to place tighter constraints on the expected extents of Si metasomatism. However, two observations indicate that regardless of conditions in a specific subduction zone, significant Si transport and alteration are likely at some point in its history. First, the region near the slab–mantle contact is likely to be a zone of concentrated shear deformation. Strong fluid focusing into shear zones can generate fluxes sufficient to cause substantial Si metasomatism. Silica metasomatism in the mantle wedge is also favoured early in the history of the subduction zone, when higher solubilities and solubility gradients will enhance advective transport (Fig. 8.1).

Si-enriched ultramafic rocks in exhumed subducted terranes are consistent with either of these scenarios. For example, ultramafic rocks in subduction-related melange from Santa Catalina Island, California, have 42–52 wt% SiO_2 and contain talc, anthophyllite, and enstatite (Bebout and Barton, 1993). Such elevated bulk Si contents require addition of silica from a fluid phase. The highly sheared nature of the lithologies suggests that the rocks may represent a permeable shear zone from near the slab–mantle interface. However, like other examples of exhumed subduction-related rocks (e.g. Ernst, 1990), the metamorphism and associated infiltration metasomatism at this locality occurred at high temperatures, early in the subduction zones' history (Grove and Bebout, 1995). Thus, this example illustrates the capacity for Si redistribution on at least a local scale in high pressure environments due to fluid focusing, high temperatures, or both.

8.6 CONCLUSIONS

The results of this analysis show that up-dip Si metasomatism in the mantle above subducting slabs is a natural consequence of the decrease in Si concentration along plausible flow paths as governed by mineral buffers. Once a steady-state mineral zonation is established in the mantle wedge, phase equilibrium constraints require the existence of regions of distinct Si concentration in the fluid. Up-dip flow in subduction zones can lead to pervasive Si metasomatism only if Darcy velocities are greater than those typical of crustal metamorphic systems. Although the range in magnitudes of Darcy velocity is poorly known in this environment, numerical estimates are consistent with at least minor Si metasomatism in the mantle wedge above long-lived, steady-state subduction zones. The extent of Si metasomatism is increased if fluid flow is focused into the shear zones likely to develop in the dynamic subduction zone environment, or when the physical conditions of subduction favour higher temperature paths than those experienced by steady-state systems.

FLUID FLOW AND TRANSPORT IN ROCKS

Mechanisms and effects

Edited by

B. Jamtveit

Department of Geology
University of Oslo

and

B. W. D. Yardley

Department of Earth Sciences
University of Leeds

CHAPMAN & HALL
London · Weinheim · New York · Tokyo · Melbourne · Madras
1997

Peacock, S. M. (1990a) Fluid processes in subduction zones. *Science*, **248**, 329–37.

Peacock, S. M. (1990b) Numerical simulation of metamorphic pressure–temperature–time paths and fluid production in subducting slabs. *Tectonics*, **9**, 1197–211.

Peacock, S. M. (1993a) The importance of blueschist → eclogite dehydration reactions in subducting oceanic slabs. *Geological Society of America Bulletin*, **105**, 684–94.

Peacock, S. M. (1993b) Large-scale hydration of the lithosphere above subducting slabs. *Chemical Geology*, **108**, 49–59.

Peacock, S. M., Rushmer, T. and Thompson, A. B. (1994) Partial melting of subducting oceanic crust. *Earth and Planetary Science Letters*, **121**, 227–44.

Sorenson, S. S. (1988) Petrology of amphibolite-facies mafic and ultramafic rocks from the Catalina Schist, southern California: metasomatism and migmatization in a subduction zone metamorphic setting. *Journal of Metamorphic Geology*, **6**, 405–35.

Sorenson, S. S. and Barton, M. D. (1987) Metasomatism and partial melting in a subduction complex: Catalina Schist, southern California. *Geology*, **15**, 115–18.

Tatsumi, Y., Hamilton, D. L. and Nesbitt, R. W. (1986) Chemical characteristics of fluid phase released from a subducted lithosphere and origin of arc magmas: evidence from high-pressure experiments and natural rocks. *Journal of Volcanology and Geothermal Research*, **29**, 293–309.

Thompson, A. B. and Connolly, J. A. D. (1992) Migration of metamorphic fluid: some aspects of mass and heat transfer. *Earth Science Reviews*, **32**, 107–21.

Walther, J. V. and Helgeson, H. C. (1977) Calculation of the thermodynamic properties of aqueous silica and the solubility of quartz and its polymorphs at high pressures and temperatures. *American Journal of Science*, **277**, 1315–51.

Wicks, F. J. and O'Hanley, D. S. (1988) Serpentine minerals: structures and petrology, in *Hydrous Phyllosilicates (Exclusive of Micas)* (ed. S.W. Bailey), Reviews of Mineralogy, **19**, 91–167.

Wyllie, P. J. and Sekine, T. (1982) The formation of mantle phlogopite in subduction zone hybridization. *Contributions to Mineralogy and Petrology*, **79**, 375–80.